Single-Shot High-Resolution Characterization of Optical Pulses by Spectral Phase Diversity

Introduction

Short optical pulses are used in many areas of optics and physics. Measuring their pulse shape became a significant technical challenge after the demonstration of mode-locking because quasi-instantaneous optical nonlinearities can yield much shorter pulses than can be directly measured via electronic processes. A large variety of strategies and diagnostics have been demonstrated to circumvent the relatively low speed of photodetectors and sampling systems,[1] but single-shot characterization of picosecond pulses remains difficult. Techniques that rely on the spatiotemporal duality are an attractive means of measuring the instantaneous power of optical pulses. Because the spectrotemporal variables (ω,t) are Fourier conjugates identical in a way to the one-dimensional (1-D) space/wave-vector coordinates (x,k), temporal imaging systems can be designed to temporally magnify the optical waveform under test and make it directly measurable via photodetection.[2,3] These imaging systems combine spectral and temporal quadratic phase modulations, the former being generally provided by dispersive materials or assemblies relying on angular dispersion, and the latter by high-bandwidth electro-optic phase modulators or nonlinear wave mixing with ancillary chirped pulses.[1] A photodiode followed by an oscilloscope can characterize the waveform under test without a significant loss of detail from the convolution by the photodetection impulse response when there is sufficient temporal magnification. Time-to-frequency conversion is an alternative to temporal magnification, where the instantaneous power of the waveform under test is mapped onto the optical spectrum of an optical pulse that can be measured with a spectrometer.

Time magnification and time-to-frequency conversion are technically elegant solutions well adapted to the telecommunication environment[4–6] but their application to the characterization of single-shot isolated events with low duty cycle is practically difficult (although not precluded). High-energy laser systems are complex large-scale optical systems that operate at a low rate (~1-h shot cycle) and generate short (1- to 100-ps) optical pulses with energy in the kilojoule range.[7] There is a significant operational complexity to accurately synchronize a subsystem that induces quadratic temporal phase modulation to the pulse under test at the end of the laser system. Such lasers require temporal diagnostics for safe operation (e.g., keeping the intensity below the damage threshold of optical components) and interpretation of experimental results (e.g., calculating the on-target intensity). A particular feature of high-energy laser systems is that the duration of the output pulse is often increased by detuning the stretcher from its optimal settings. This allows for safe amplification and recompression of pulses at higher energy levels because the fluence damage threshold of optical components, in particular diffraction gratings, depends strongly on the pulse duration. In these conditions, the pulse duration must be monitored accurately to avoid amplifying pulses that are shorter than expected to unsafe energy levels. Because of the large scale of these laser systems, the measurement conditions are often nonideal—e.g., wavefront distortions and pointing variations at the end of the system can make it difficult to implement diagnostics based on free-space nonlinear interactions.

This article describes a temporal diagnostic analogous to the phase-diversity technique used for wavefront metrology[8,9] and demonstrates it in the context of pulse characterization on a high-energy chirped-pulse–amplification (CPA) laser system. The spectral phase-diversity technique allows for characterization of a coherent optical pulse that is shorter than the photodetection impulse response. A single-mode fiber in the near field of the beam couples the pulse under test into the fiber-based diagnostic, therefore alleviating the impact of wavefront and pointing variations. Precise synchronization is not required because of the long memory length of commercial oscilloscopes. The diagnostic principle is described in the next section, followed by the experimental implementation and algorithms, and the experimental results obtained on the OMEGA EP laser.[10]

Principle

The spectral phase-diversity technique is analogous to the spatial phase-diversity technique used to characterize the wavefront $\varphi(x,y)$ of a coherent beam with fluence distribution

$F(x,y)$ in the near field [Fig. 144.9(a)]. In this technique, the beam to be characterized is focused and fluence distributions are measured at various longitudinal positions in the far field.[9] The measured fluence distributions G_k are expressed in the far-field coordinates system (x', y') by

$$G_k(x',y') = \left| \mathrm{FT}\left\{ \sqrt{\mathrm{F}(x,y)}\, \exp\left[i\varphi(x,y)\right] \exp\left[-i\frac{\pi \Delta z_k}{\lambda f^2}\left(x^2+y^2\right)\right]\right\}\right|^2, \quad (1)$$

where FT is the Fourier transform, λ is the wavelength, f is the focal length of the focusing element, and Δz_k represents the distance offsets in the longitudinal direction. The input spatial phase is reconstructed by processing the set of measured fluence distributions. There are many reconstruction approaches in spatial phase diversity, for example, by parametrization of the unknown phase or by projection on a basis such as Legendre polynomials. The unknown wavefront is obtained by minimizing an error metric quantifying the difference between the measured and calculated sets of fluence distributions.

Spectral phase diversity is based on the duality between the spectrotemporal variables (ω,t) and the spatial variables (x,k). The spectral phase $\varphi(\omega)$ of the input field is reconstructed using the instantaneous powers $P_k(t)$ that are measured after known spectral phases $\psi_k(\omega)$ have been introduced [Fig. 144.9(b)]. The optical spectrum of the pulse, $S(\omega)$, is assumed to be accurately measured because spectral density measurements pose no significant technical difficulty and are routinely performed. (Equivalently, it is routine to measure the fluence beam profile of the beam to be characterized for wavefront measurements via spatial phase diversity.) One significant practical difference with spatial phase diversity is that temporal measurements are convolutions of the actual instantaneous power with the photodetection impulse response R, leading to the measured data set

$$P'_k = P_k \otimes R \quad (2)$$

with

$$P'_k(t) = \left| \int \sqrt{S(\omega)}\, \exp\left\{ i\left[\varphi(\omega)+\psi_k(\omega)+\omega t\right]\right\} \mathrm{d}\omega \right|^2. \quad (3)$$

Equation (3) is a 1-D equivalent of Eq. (1) when the induced spectral phases are quadratic functions of the optical frequency ω. Reconstruction of the unknown φ from the known S, ψ_k, R, and P'_k is a minimization problem. For our application, we chose the parametrization of the spectral phase with its second-order and third-order terms in the Taylor expansion around the central frequency of the pulse $\varphi(\omega) = \varphi_2\omega^2/2 + \varphi_3\omega^3/6$. This adequately represents the pulse-shape variations that must be characterized when tuning the stretcher of the CPA systems to adjust the output-pulse duration. We found that the measured data were consistent with essentially zero third-order dispersion because the stretcher and compressor of each CPA system had already been matched accurately; therefore, the results presented here correspond to parametrizing the spectral phase with only its second-order coefficient. This is evidently not a limitation of spectral phase diversity because the technique, like its spatial counterpart, can in principle be applied with any parametrization basis provided that the data (measured set of power versus time $\{P'_k\}$ and optical spectrum) can unambiguously be linked to a set of parameters with sufficient accuracy and precision for the targeted application.

When ψ_k is a quadratic function inducing relatively small changes to the input pulse shape, Eq. (3) can be developed to yield the temporal transport-of-intensity equation.[11] This equation links the dispersion-induced changes in the time-varying

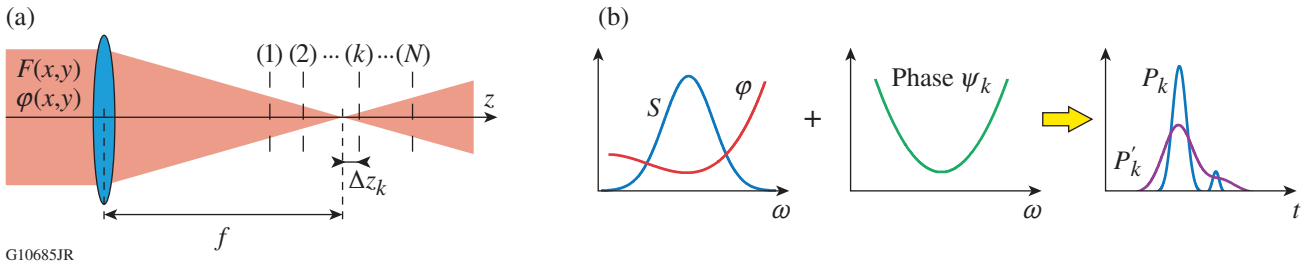

Figure 144.9
(a) Principle of spatial phase diversity for wavefront measurements and (b) temporal phase diversity for optical pulse characterization. In (a), the spatially resolved fluence $G_k(x,y)$ is measured at various longitudinal locations Δz_k close to the focus to reconstruct the near-field phase $\varphi(x,y)$. In (b), various amounts of spectral phase ψ_k are introduced on the pulse under test, yielding the instantaneous power $P_k(t)$, and the spectral phase $\varphi(\omega)$ is reconstructed from the powers $P'_k(t)$ measured after photodetection with response $R(t)$.

power of an optical field to its temporal phase. It has been used to temporally characterize nonlinear phase shifts[11] and optical pulses after temporal stretching to allow for accurate photodetection.[12] The experimental data presented in this article have a relatively low sampling rate and signal-to-noise ratio compared to the data of Refs. 11 and 12 obtained on repetitive signals with a sampling oscilloscope; an error minimization strategy appears more suitable, although it is not based on a direct analytic data inversion and requires more computing power.

Setup and Algorithm

The fiber-based experimental setup for spectral phase diversity is described in Fig. 144.10. The input pulse propagates in a custom-built fiber assembly composed of multiple sequentially connected 2×2 fiber splitters. One output port of splitter j and one input port of splitter $j + 1$ are connected by a short optical fiber. The other pair of ports is connected by a delay fiber with length $l \times 2^{j-1}$. The fiber assembly (seven splitters, $l = 4$ m) generates $N = 64$ output pulses with an interpulse delay $\tau = 20$ ns. The fiber assembly serves two purposes. The first purpose is to delay the output pulses relative to each other so that their instantaneous power can be measured with a single photodiode and a single-channel oscilloscope. This property has been used with similar fiber assemblies to increase the photodetection single-shot signal-to-noise ratio for narrowband optical pulses. For narrowband pulses, the output-pulse shapes are essentially identical and can be summed up after photodetection to provide a lower-noise determination of the input-pulse shape.[13,14] Chromatic dispersion in the optical fibers induces changes in the spectral phase and, subsequently, the instantaneous power of broadband optical pulses. The second purpose of the fiber assembly is to induce different amounts of chromatic dispersion by propagation in different fiber lengths. The chromatic dispersion of single-mode fiber at 1053 nm is approximately –40 ps/nm/km ($\varphi_2 > 0$), leading to a relative dispersion of –0.16 ps/nm between successive output pulses and non-negligible pulse-shape changes for a pulse with a bandwidth of the order of a few nanometers or larger. One of the fiber-assembly outputs is connected to a high-bandwidth InGaAs photodiode (DSC10, Discovery Semiconductors) and a real-time high-bandwidth oscilloscope. We tested two oscilloscopes for this application, a 45-GHz Teledyne Lecroy Wavemaster 8Zi-A and a 70-GHz Tektronix DPO77002SX, leading to photodetection impulse responses at low power levels with a full width at half maximum (FWHM) of 17 ps and 13.5 ps, respectively. The oscilloscopes nominally have a flat frequency response over their stated bandwidth, and the impulse response is limited mainly by the photodiode. The two oscilloscopes have a record length much longer than the ~1.3-μs temporal extent of the 64 pulses with 20-ns interpulse delay. The oscilloscopes were triggered either on the signal itself or with an external trigger synchronized to the pulse under test. The single-shot characterization of isolated optical pulses generated by a high-energy laser system requires a real-time oscilloscope, but the diagnostic can be operated with a sampling oscilloscope if the source under test delivers a train of identical optical pulses that are separated by more than the temporal extent of the fiber-assembly output. Two optical pulses coupled to the two inputs of the first fiber splitter can be characterized independently in a single shot provided that the 64 pulses that are generated by each input pulse do not temporally overlap, or equivalently, that the two input pulses do not temporally overlap at the first fiber splitter. This condition is easily met in practice, and optical fiber can be added to one input in the unlikely event that the pulses overlap. The possibility of characterizing two independent optical pulses with a single setup is advantageously put into practice to characterize the outputs of the two OMEGA EP CPA beamlines.[10]

An example of photodetection impulse response measured with a subpicosecond mode-locked laser is shown in Fig. 144.11(a), where the typical noise level (~10% peak-to-valley relative to the full voltage range) and relatively low sampling rate (120 GS/s, i.e., one sample every 8.25 ps) can be

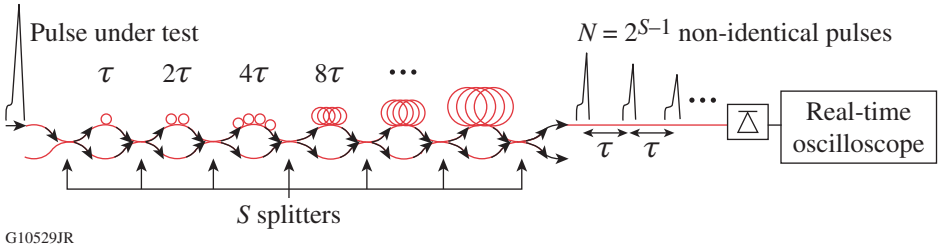

Figure 144.10
Setup for spectral phase diversity, based on a fiber assembly and photodetection. The 2×2 splitters combined with dispersive delay fibers generate 2^{S-1} pulses that are photodetected at one output of the assembly, where S is the number of splitters.

seen. Figure 144.11(b) shows that the duration of the impulse response increases with increasing incident power because of nonlinearities in the photodetector.[15,16] Figure 144.11(c) shows that the measured FWHM varies by only a few picoseconds over a large range of pulse durations that can be generated by our laser system. Measurement noise, a low sampling rate, and variations in impulse response render the task of directly deconvolving measured data to retrieve the optical pulse shape impractical for pulses shorter than the impulse response.

Examples of spectral phase-diversity data measured for an input pulse close to best compression and a chirped pulse are shown in the upper and lower rows of Fig. 144.12, respectively. An input pulse with negligible spectral-phase distortions yields chirped output pulses, with chromatic dispersion and temporal extent increasing with the fiber length in which they have propagated (upper row). An input pulse with negative second-order dispersion experiences recompression in the fiber assembly, yielding some output pulses close to the Fourier-transform limit

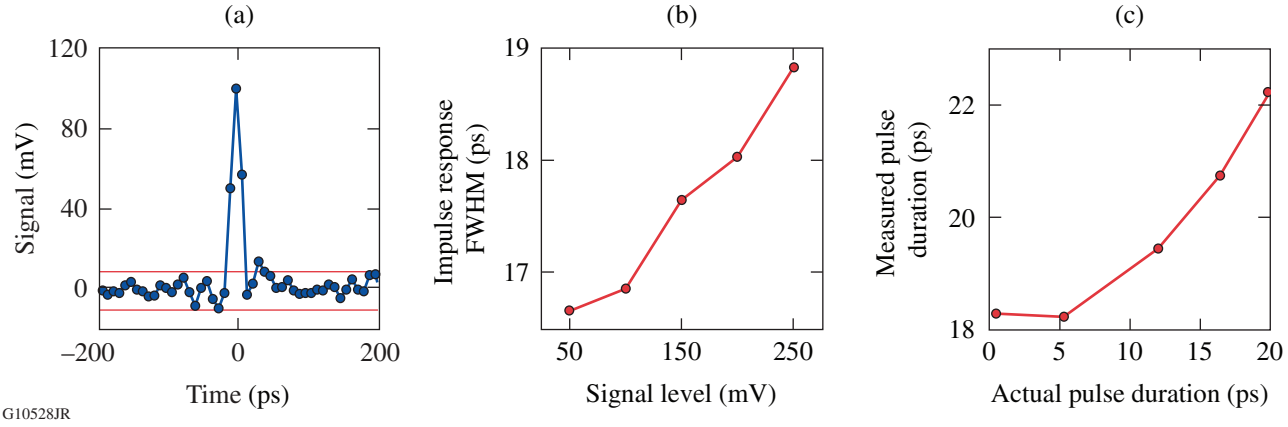

Figure 144.11
(a) An example of measured impulse response with the DSC10 photodetector and Lecroy 45-GHz oscilloscope; (b) measured full width at half maximum (FWHM) of the impulse response versus signal level; (c) measured FWHM of an optical pulse versus calculated FWHM when the OMEGA EP stretcher is detuned.

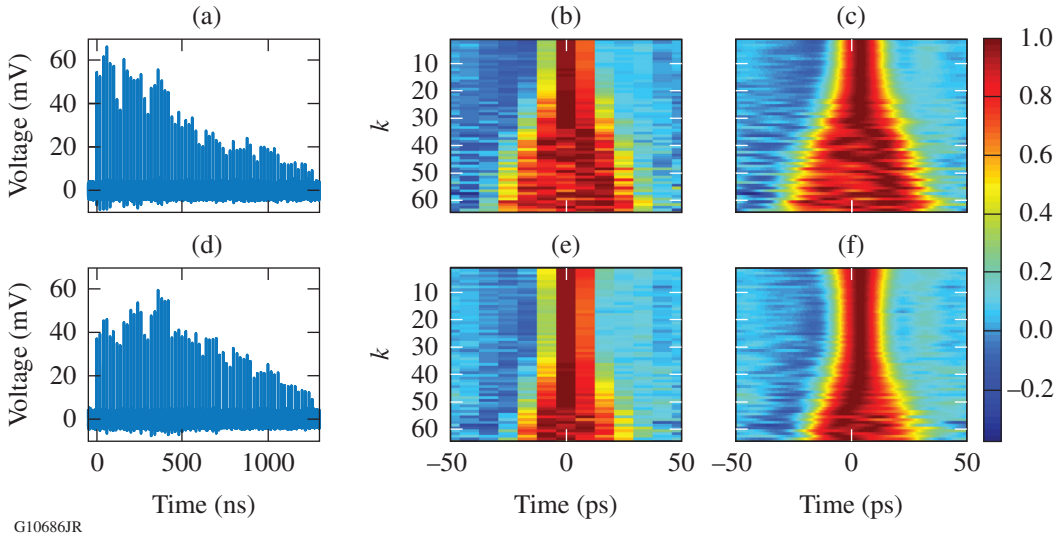

Figure 144.12
Examples of experimental data for a pulse close to best compression (upper row) and after stretcher detuning (lower row). [(a),(d)] Waveform measured by the oscilloscope; [(b),(e)] composite trace composed of the power versus time data for the 64 output pulses after retiming; [(c),(f)] power versus time for the 64 output pulses oversampled 32 times by zero padding for display purposes.

(lower row). An input pulse with positive second-order dispersion is further stretched in the fiber assembly (not shown). The experimental data intuitively indicate the sign and approximate amount of the input-pulse chromatic dispersion from an understanding of the properties of the fiber assembly.

The input-pulse dispersion was determined by comparing the measured data; i.e., the set of instantaneous powers $\{P'_{k,\,\mathrm{meas}}\}$, to the set of instantaneous powers $\{P'_{k,\,\mathrm{calc}}\}$ calculated with a given set of parameters (e.g., second-order and third-order dispersion), the known optical spectrum, chromatic dispersion of the optical fiber, and photodetection impulse response. A Gaussian impulse response with FWHM equal to the extrapolated FWHM of the measured impulse response at a low power level was consistently used. An error metric ε between the two data sets is defined by

$$\varepsilon = \sqrt{\sum_k \varepsilon_k^2}$$

$$= \sqrt{\sum_k \int \mathrm{d}t \left[P'_{k,\,\mathrm{meas}}(t) - P'_{k,\,\mathrm{calc}}(t-\tau_k)\right]^2 \Big/ 2}, \qquad (4)$$

where each ε_k is minimized over the delay τ_k, which takes into account timing shifts containing no meaningful information on the pulse shape. For each ε_k, the instantaneous powers are normalized by

$$\int \mathrm{d}t P'_{k,\,\mathrm{meas}}(t)^2 = \int \mathrm{d}t P'_{k,\,\mathrm{calc}}(t)^2 = 1.$$

By definition, $\varepsilon_k = 0$ means that the two functions are identical and $\varepsilon_k = 1$ means that their temporal overlap is zero. With this normalization, the minimal value of ε_k is $\sqrt{1-0_{k,\max}}$, where $0_{k,\max}$ is the value of the overlap integral:

$$0_k(\tau) = \int \mathrm{d}t P'_{k,\,\mathrm{meas}}(t)\, P'_{k,\,\mathrm{calc}}(t-\tau)$$

maximized over τ. The error ε_k can be calculated in a computationally efficient manner because each $0_{k,\max}$ is simply the maximum value of the Fourier transform of 0_k. Figure 144.13 shows ε as a function of the input φ_2, assuming $\varphi_3 = 0$, and as a function of φ_2 and φ_3 for the lower-row dataset of Fig. 144.12. The error is clearly minimized for a single set of input-pulse parameters. As previously stated, the retrieved φ_3 was consistently insignificantly close to 0; therefore, all further data presented in this article were obtained by error minimization over φ_2 only. Once spectral-phase parameters are identified, the input pulse shape is calculated by Fourier transformation.

Experimental Results

1. Laser Description

The phase-diversity diagnostic has been tested on OMEGA EP. The two short-pulse beamlines can deliver amplified optical pulses with durations ranging from subpicosecond to 100 ps. The output-pulse duration is adjusted on each system by detuning the single-grating Offner-triplet stretcher.[17] Its spherical mirrors are mounted on a rail and can be translated relative to the stretcher grating while keeping the intermirror distance constant. Each beamline has an optical parametric chirped-pulse–amplification (OPCPA) front end that amplifies the stretched output of a mode-locked laser (~6-nm FWHM). Saturation in the two parametric-amplifier stages leads to a flattop spectrum (FWHM ~7.5 nm) (Ref. 18).

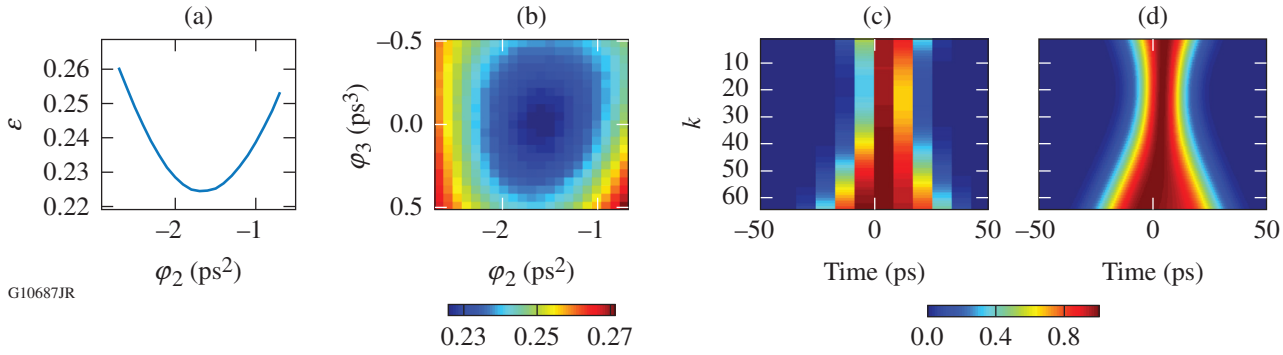

Figure 144.13
Examples of phase retrieval for the lower-row data of Fig. 144.12. (a) Error versus input second-order dispersion; (b) error versus input second-order and third-order dispersion; [(c),(d)] calculated 64-pulse composite trace with the determined φ_2 at the sampling rate of the oscilloscope and oversampled by a factor of 32 with zero padding.

Most experimental results presented in this article correspond to the single-shot characterization of the OPCPA pulse after propagation through an entire OMEGA EP beamline and recompression. For statistical purposes, ten acquisitions are performed at each set of experimental settings, e.g., stretcher detuning. The pulse under test is coupled in the fiber assembly by a single-mode fiber at an image plane where the beam has a high-order super-Gaussian square profile. The energy required for accurate characterization is typically 50 pJ in the input fiber, which corresponds to ~5 μJ in the free-space beam. Reducing the beam size or focusing into the fiber could increase the sensitivity of the diagnostic, but this might come at the expense of increased sensitivity to beam pointing and wavefront variations.

2. Front-End Pulse Characterization

Figure 144.14 displays experimental results obtained for pulse durations ranging from best compression (~500-fs pulse) to 20 ps. The retrieved second-order dispersion and duration agree very well with the stretcher model based on design parameters (groove density = 1740 l/mm, angle of incidence = 72.5°) except for pulses close to best compression (~2 ps and shorter), where the magnitude of the retrieved second-order dispersion and pulse duration are overestimated. This effect appears to be almost negligible very close to best compression, where the retrieved pulse duration (600 fs) is close enough to the Fourier-transform pulse duration (~400 fs) and well within the targeted range allowable for our application. Small modulations of the optical spectrum resulting from self-phase modulation (SPM) were identified for this range of input-pulse durations.

Figure 144.15 presents results taken in the dispersion region around –1.73 ps^2. This dispersion value corresponds to an on-shot pulse duration of 10 ps, taking into account the gain narrowing in Nd:glass amplifiers that decreases the optical bandwidth from ~7.5 nm to ~3.5 nm. This regime is highly

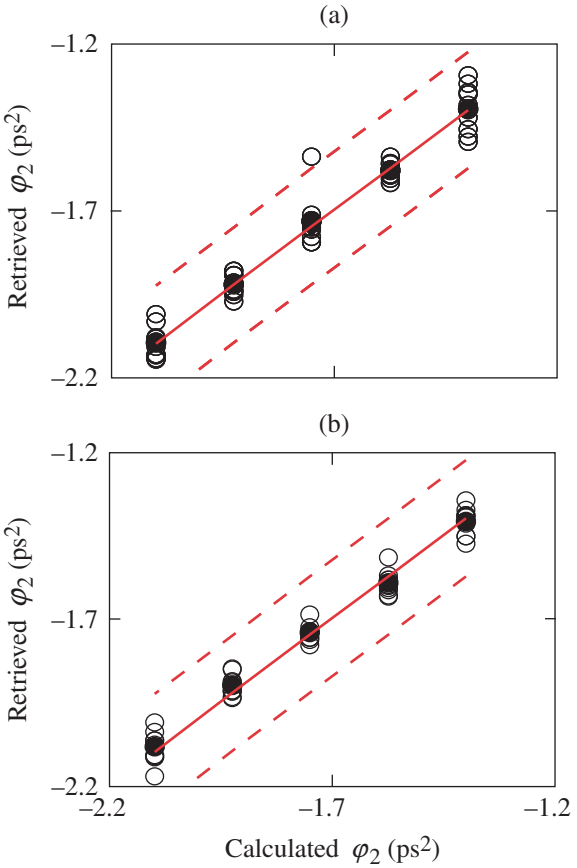

Figure 144.15
Retrieved φ_2 versus calculated φ_2 for (a) the 45-GHz oscilloscope and (b) the 70-GHz oscilloscope. On each plot, the simulated φ_2 is plotted with a solid red line, a 10% margin is plotted with a dashed red line, and the solid circles correspond to the average of the ten single-shot determinations plotted with open circles for each stretcher setting.

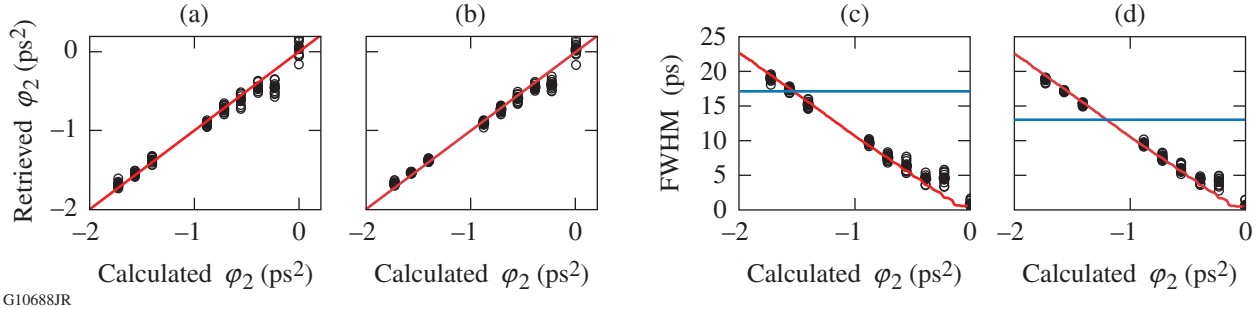

Figure 144.14
(a) and (b) Retrieved φ_2 and [(c),(d)] FWHM versus calculated stretcher dispersion. (a) and (c) correspond to data obtained with the Lecroy 45-GHz oscilloscope. (b) and (d) correspond to data obtained with the Tektronix 70-GHz oscilloscope. Simulated values are plotted with a red line. The FWHM of the impulse response of each oscilloscope is shown in blue on the respective plots.

relevant operationally because the maximum energy for safe operation at this pulse duration is significantly higher than at best compression; therefore, a large fraction of scientific shots are performed at 10 ps. The measured data are very consistent with the system model, and there is little spread of the retrieved dispersion around the calculated value. Over the range of stretcher dispersions shown in Fig. 144.15, the root mean square (rms) and peak-to-valley precision are 0.05 ps^2 and 0.15 ps^2, respectively, for the 45-GHz oscilloscope. They are slightly better with the higher-bandwidth, 70-GHz oscilloscope, with rms and peak-to-valley precision of 0.03 ps^2 and 0.12 ps^2, respectively. The higher precision is attributed to the slightly better intrinsic noise performance of the latter oscilloscope compounded with the shorter impulse response. A 10% change in pulse duration around this stretcher setting corresponds to 0.17 ps^2. This indicates that pulse reconstruction with precision better than 10% can be obtained on a single-shot basis with this diagnostic.

On-Shot Pulse Characterization

The data retrieved by spectral phase diversity are compared in Fig. 144.16 to results from two currently deployed diagnostics. Figure 144.16(a) displays a single-shot autocorrelation measured when the stretcher is set to obtain the shortest pulse achievable on the system. This autocorrelation is compared to an autocorrelation calculated with the measured optical spectrum and retrieved dispersion, demonstrating that the best-compression stretcher setting has been identified with subpicosecond precision. Figures 144.16(b) and 144.16(c) compare the instantaneous power measured by a streak camera with the power reconstructed with the spectral phase-diversity diagnostic. This comparison was performed on amplified OMEGA EP shots, for which the stretcher was set to yield either a 5-ps pulse or a 12-ps pulse, taking into account the gain narrowing in the Nd:glass amplifiers to ~3.5 nm. Satisfactory agreement was obtained, considering the significant operational complexity and sources of uncertainty associated with the streak camera.[19]

Conclusions

We have demonstrated a diagnostic based on the concept of spectral phase diversity to characterize picosecond optical pulses with fast photodetection. The experimental trace consists of the photodetected instantaneous power of optical pulses derived from the pulse under test by adding known amounts of chromatic dispersion. An error minimization algorithm retrieves the spectral phase that best matches the measured data, taking into account the diagnostic parameters. The single-shot, fiber-coupled diagnostic has been demonstrated in the context of stretcher tuning for a high-energy laser system and shows good performance over a large range of pulse durations including pulses several times shorter than the photodetection impulse response.

Improved diagnostic performance is expected from technological advances in high-bandwidth photodiodes, high-bandwidth real-time oscilloscopes, and optimization of the fiber assembly used to implement spectral phase diversity. We are currently using simulations to study the impact of the fiber-assembly parameters on the diagnostic performance and the ability of spectral phase diversity to characterize more-general pulse shapes than those encountered at the output of a chirped-pulse–amplification system.

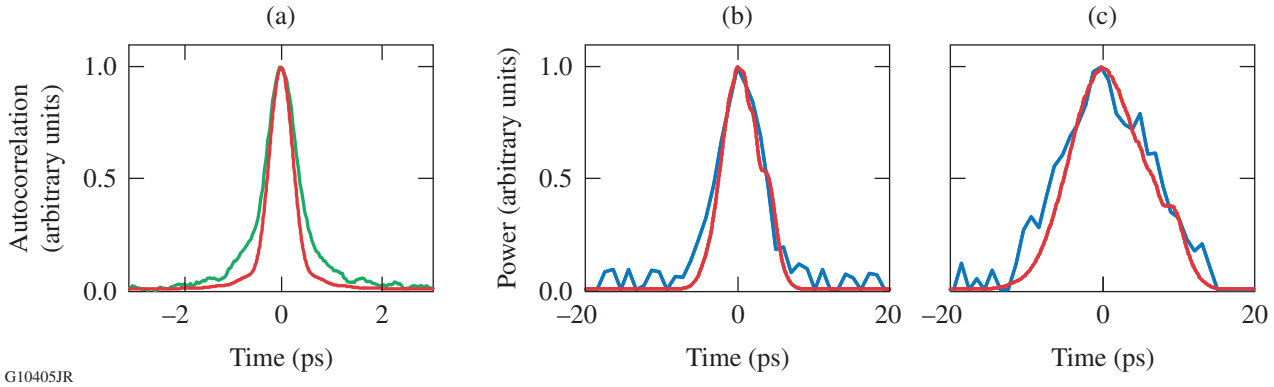

Figure 144.16
Comparison of measurements performed with the spectral phase-diversity diagnostic (red line), a single-shot autocorrelator [green line in (a)], and a streak camera [blue line in (b) and (c)]. For (a), an OPCPA pulse is characterized at the output of OMEGA EP when the stretcher was set at the best-compression position. For (b) and (c), Nd:glass amplifiers were fired and the stretcher was set for a 5-ps or 12-ps amplified output pulse, respectively.

ACKNOWLEDGMENT

The authors thank R. Cuffney for manufacturing the fiber assembly used for the experiments and Tektronix for the loan of the DPO77002SX oscilloscope. This material is based upon work supported by the Department of Energy National Nuclear Security Administration under Award Number DE-NA0001944, the University of Rochester, and the New York State Energy Research and Development Authority. The support of DOE does not constitute an endorsement by DOE of the views expressed in this article.

REFERENCES

1. I. A. Walmsley and C. Dorrer, Adv. Opt. Photon. **1**, 308 (2009).
2. P. Tournois, J.-L. Vernet, and G. Bienvenu, C. R. Acad. Sc., Ser. B (Paris) **267**, 375 (1968).
3. B. H. Kolner, IEEE J. Quantum Electron. **30**, 1951 (1994).
4. M. T. Kauffman *et al*., Appl. Phys. Lett. **64**, 270 (1994).
5. C. V. Bennett and B. H. Kolner, Opt. Lett. **24**, 783 (1999).
6. R. Salem *et al*., Opt. Lett. **33**, 1047 (2008).
7. J. D. Zuegel, S. Borneis, C. Barty, B. LeGarrec, C. Danson, N. Miyanaga, P. K. Rambo, C. LeBlanc, T. J. Kessler, A. W. Schmid, L. J. Waxer, J. H. Kelly, B. Kruschwitz, R. Jungquist, E. Moses, J. Britten, I. Jovanovic, J. Dawson, and N. Blanchot, Fusion Sci. Technol. **49**, 453 (2006).
8. R. A. Gonsalves, Opt. Eng. **21**, 829 (1982).
9. S.-W. Bahk, J. Bromage, I. A. Begishev, C. Mileham, C. Stoeckl, M. Storm, and J. D. Zuegel, Appl. Opt. **47**, 4589 (2008).
10. D. N. Maywar, J. H. Kelly, L. J. Waxer, S. F. B. Morse, I. A. Begishev, J. Bromage, C. Dorrer, J. L. Edwards, L. Folnsbee, M. J. Guardalben, S. D. Jacobs, R. Jungquist, T. J. Kessler, R. W. Kidder, B. E. Kruschwitz, S. J. Loucks, J. R. Marciante, R. L. McCrory, D. D. Meyerhofer, A. V. Okishev, J. B. Oliver, G. Pien, J. Qiao, J. Puth, A. L. Rigatti, A. W. Schmid, M. J. Shoup, III, C. Stoeckl, K. A. Thorp, and J. D. Zuegel, J. Phys.: Conf. Ser. **112**, 032007 (2008).
11. C. Dorrer, Opt. Lett. **30**, 3237 (2005).
12. C. Cuadrado-Laborde *et al*., Opt. Lett. **39**, 598 (2014).
13. J. R. Marciante, W. R. Donaldson, and R. G. Roides, IEEE Photonics Technol. Lett. **19**, 1344 (2007).
14. C. Dorrer, J. Lightwave Technol. **31**, 1374 (2013).
15. K. J. Williams and R. D. Esman, IEEE Photonics Technol. Lett. **10**, 1015 (1998).
16. T. S. Clement *et al*., in *Technical Digest: Symposium on Optical Fiber Measurements, 2000*, edited by P. A. Williams and G. W. Day, NIST (U.S.) Special Publication 953 (National Institute of Standards and Technology, Boulder, CO, 2000), pp. 121–124.
17. G. Chériaux *et al*., Opt. Lett. **21**, 414 (1996).
18. C. Dorrer, A. Consentino, D. Irwin, J. Qiao, and J. D. Zuegel, J. Opt. A: Pure Appl. Opt. **17**, 094007 (2015).
19. J. Qiao, P. A. Jaanimagi, R. Boni, J. Bromage, and E. Hill, Rev. Sci. Instrum. **84**, 073104 (2013).